J Ther Eng, Vol. 11, No. 2, pp. 422–433, March, 2025

Journal of Thermal Engineering
Web page info: https://jten.yildiz.edu.tr
DOI: 10.14744/thermal.0000924

Research Article

# Enhancing aerodynamic efficiency with a moving surface panel on a NACA 2412 airfoil

**Ravichandrakumar Kumar BHASKAR[1,*], Ganapathy Subramanian L. R.[1]**

[1]*Department of Aerospace Engineering, SRM Institute of Science and Technology, SRM Nagar, Tamil Nadu, 603 203, India*

## ARTICLE INFO

*Article history*
Received: 28 July 2024
Revised: 29 November 2024
Accepted: 23 December 2024

**Keywords:**
Airfoil; Flow Control Techniques; Flow Separation & Aerodynamic Performance; Fluid Flow; Moving Surface Boundary

## ABSTRACT

This study investigates the application of a moving surface boundary on a NACA 2412 airfoil using a belt mechanism with two pulleys to enhance aerodynamic efficiency. By accelerating the airflow, the moving surface helps delay flow separation, which typically limits aerodynamic performance. Previous computational works simplified the moving surface as a flat panel, often neglecting the gap between the panel and airfoil, as well as the complexities introduced by the belt-pulley mechanism. Building on earlier research, this study models a belt mechanism that spans 20% of the airfoil's chord length, evaluating its aerodynamic impact at different chord-wise locations. Numerical analysis was conducted at varying belt speeds and panel positions. Results showed that placing the panel at 20% and 40% of the chord, as well as near the leading edge, yielded the best performance, increasing aerodynamic efficiency by 153%, 159%, and 166%, respectively. These enhancements were particularly evident at lower angles of attack, especially around 4 degrees. The novelty of this work lies in its realistic representation of the belt mechanism, accounting for gaps and flow disturbances caused by the pulleys. This approach provides a more accurate simulation of real-world applications, with findings suggesting that placing the moving surface at 20% chord length offers optimal aerodynamic gains, offering valuable insights for future flow control applications.

**Cite this article as:** Bhaskar RK, L. R. GS. Enhancing aerodynamic efficiency with a moving surface panel on a NACA 2412 airfoil. J Ther Eng 2025;11(2):422–433.

## INTRODUCTION

The movable surface boundary control method has been widely recognized as a promising technique to manage or delay flow separation, improving aerodynamic efficiency. Historically, this has been achieved by the utilization of rotating hollow cylinders. Initial studies by [1] and [2] indicated that rotating cylinders positioned at the leading edges associated with airfoils might significantly improve aerodynamic efficiency. This concept evolved, with researchers like [3] applying movable surface boundary control to various shapes, while [4] explored its effectiveness in underwater vehicles. Computational methods gained traction in the early 2000s, with studies like [5, 6] simulating improved airfoil performance, and [7] focusing on drag reduction in bluff bodies.

In the last few years, advancements in flow control technologies and computational models have enabled more

---

***Corresponding author.**
*E-mail address: ravicham@srmist.edu.in

*This paper was recommended for publication in revised form by Editor-in-Chief Ahmet Selim Dalkılıç*

Published by Yıldız Technical University Press, İstanbul, Turkey

refined applications. [8] explored the Magnus effect, [9] enhanced the NACA 0012 airfoil's characteristics of lift and drag, and [10] investigated rotating elliptic cylinders to alter flow patterns. More recent efforts, such as those by [11, 12] focused on optimizing symmetrical airfoils and managing flow separation with spinning cylinders. [13] extended this by enhancing lift and drag with innovative airfoil designs. [14] has explored optimal design in airfoil with leading edge rotating cylinder. Leading edge rotating cylinder is also explored in wind turbines shows improved performance [15]. However, despite these advances, most studies continue to rely on the use of rotating cylinders, which, while effective, occupy significant space and may not be practical for certain real-world applications.

There is a limited exploration of belt mechanisms as a method for moving surface boundary control. Unlike rotating cylinders, belt mechanisms offer a larger moving surface area. [16] investigate the effects of using a moving-wall boundary condition to enhance lift generation on a low aspect ratio airfoil. The study explores how a moving surface influences flow separation and the overall aerodynamic performance, demonstrating that a moving wall can significantly improve lift characteristics by delaying boundary layer separation. The results provide insights into potential applications of this technique in improving the efficiency of airfoils in various engineering fields. Collectively, Salimipour's computational work demonstrates the significant potential of moving surface techniques in enhancing aerodynamic performance across a variety of applications. His research covers a broad range of topics, including the optimization of airfoils [17] and wind turbine blades [18], where moving surfaces were shown to substantially improve the lift-to-drag ratio and overall aerodynamic efficiency. Additionally, studies on elliptic moving belts [19] and circular cylinders [20] reveal the effectiveness of these surfaces in reducing drag, minimizing vortex losses, and conserving power. His investigations into transitional flow regimes [21] provide valuable insights into control strategies for managing complex flow dynamics, further highlighting the versatility and applicability of moving surfaces in various engineering fields. Collectively, these works highlight the versatility and potential of moving surfaces as a moving panel in optimizing performance across various applications. However, these studies also used a simplified model without accounting for the detailed dynamics of a belt system integrated into an airfoil. The moving surfaces have largely been represented as simplified flat panels in simulations, omitting the impact of gaps between the moving panel and the airfoil as well as the flow complexities introduced by the pulleys. This simplification overlooks key factors that could influence the overall aerodynamic performance and the effectiveness of the moving-wall flow control method.

There is need for a more comprehensive analysis of a belt mechanism that accurately simulates its real-world application, including the gaps and pulleys, which could introduce flow disturbances. This study seeks to identify the ideal positioning of a movable surface panel on a NACA 2412 airfoil, evaluating its aerodynamic and mechanical performance at various chord-wise locations and different cylinder speed ratios (CSRs) across multiple Angle of Attack (AOA). By doing so, this work goes beyond previous efforts by providing a more realistic assessment of how belt systems influence aerodynamic performance, potentially leading to more efficient flow control solutions for airfoils.

## METHODOLOGY

### Geometry

The study uses an asymmetrical NACA 2412 airfoil model as its foundation. The model includes a Moving Panel (MP) that has a fixed length equal to 20% of the airfoil chord . Additionally, the MP model incorporates a belt system consisting of two rollers with a diameter of 0.025C. The MP is positioned at three distinct locations along the chord by aligning the LE of the MP with the airfoil's LE, 20% of the chord length (0.2C), and 40% of the chord length (0.4C), as shown in Figure 1.

This is done so that when the AOA is high, the flow separation can be delayed. The flow analysis will be conducted at a Reynolds number (Re) of 2.2 x$10^6$ at various places, using varying CSR of 0, 1, 2, and 3. This work has utilized the real belt mechanism to understand the consequences resulting from the distance between stators and moving bodies.

### Numerical Formulation

The study is conducted on objects in motion, allowing for precise predictions using the 2D Unsteady Reynolds Average Navier Stoke›s equation model. The equations include continuity, momentum, and energy. Moreover, Transition SST(Shear Stress Transport) turbulence model is used to improve the accuracy of predicting the flow near the wall.

Continuity equation:

$$\frac{\partial \overline{v_x}}{\partial x} + \frac{\partial \overline{v_y}}{\partial y} = 0 \tag{1}$$

X-momentum equation:

$$\frac{\partial \overline{v_x}}{\partial t} + \overline{v_x}\,\frac{\partial \overline{v_x}}{\partial x} + \overline{v_y}\,\frac{\partial \overline{v_x}}{\partial y} + \frac{1}{\rho}\frac{\partial \bar{p}}{\partial x} = v\left[\frac{\partial^2 \overline{v_x}}{\partial x^2} + \frac{\partial^2 \overline{v_x}}{\partial y^2}\right] - \left[\frac{\partial^2 \overline{(v_x{}' v_x{}')}}{\partial x} + \frac{\partial^2 \overline{(v_x{}' v_y{}')}}{\partial y}\right] \tag{2}$$

Y-momentum equation:

$$\frac{\partial \overline{v_y}}{\partial t} + \overline{v_x}\,\frac{\partial \overline{v_y}}{\partial x} + \overline{v_y}\,\frac{\partial \overline{v_y}}{\partial y} + \frac{1}{\rho}\frac{\partial \bar{p}}{\partial y} = v\left[\frac{\partial^2 \overline{v_y}}{\partial x^2} + \frac{\partial^2 \overline{v_y}}{\partial y^2}\right] - \left[\frac{\partial^2 \overline{(v_x{}' v_y{}')}}{\partial x} + \frac{\partial^2 \overline{(v_y{}' v_y{}')}}{\partial y}\right] \tag{3}$$

Energy equation:

$$\rho\left[\frac{\partial \bar{T}}{\partial t} + \overline{v_x}\frac{\partial \bar{T}}{\partial x} + \overline{v_y}\frac{\partial \bar{T}}{\partial y}\right] = \rho\dot{q} + \frac{\partial}{\partial x}\left(k_T\frac{\partial \bar{T}}{\partial x}\right) + \frac{\partial}{\partial y}\left(k_T \cdot \frac{\partial \bar{T}}{\partial y}\right) \tag{4}$$

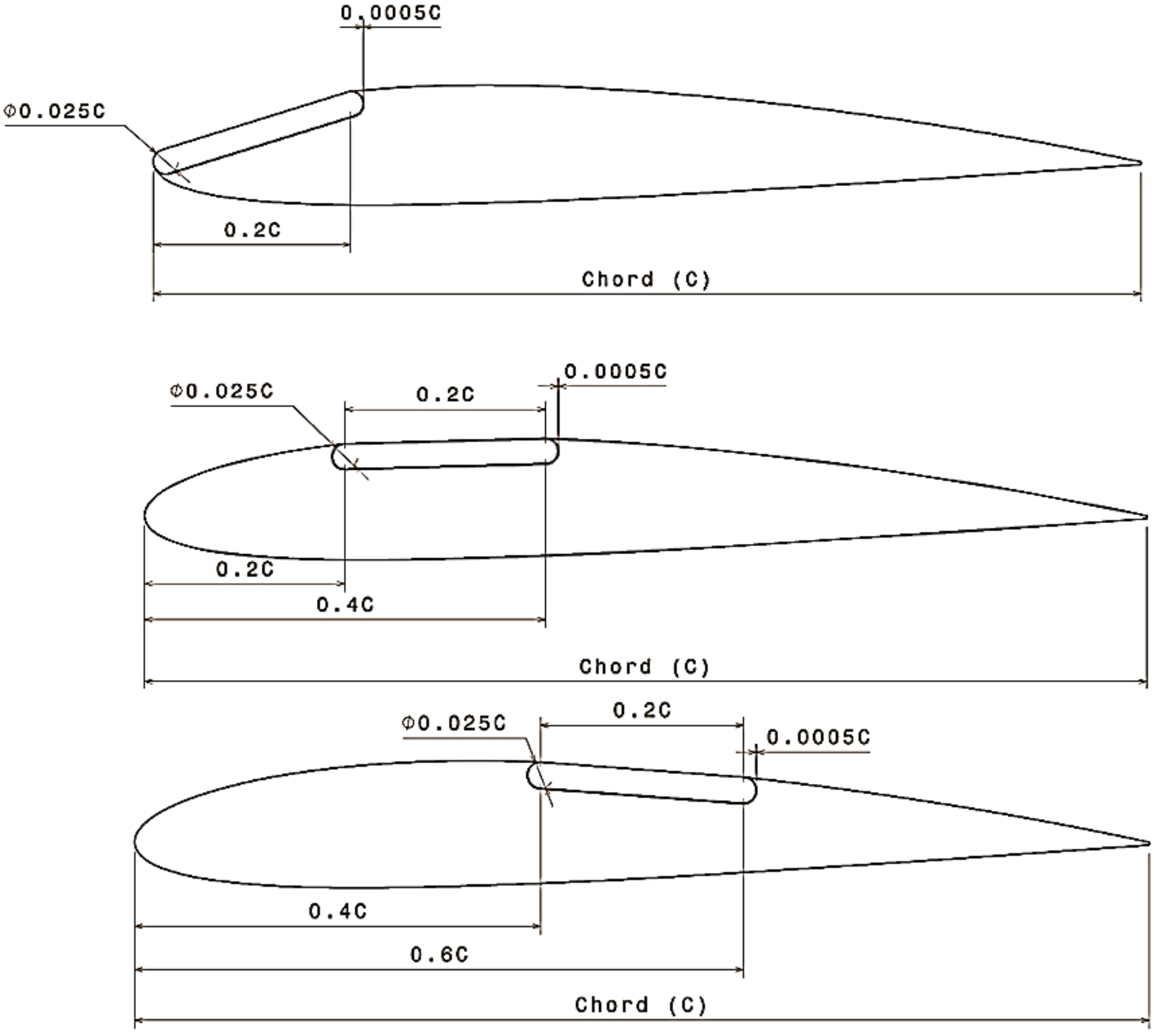

**Figure 1.** NACA2412 with different positions of moving surface panel (MP), a) MP at LE, b) MP at 0.2C, c) MP at 0.4C.

In transition SST, where the K-ω-SST equation, along with the intermittency equation and transition onset criterion equation, are merged. In ANSYS, the turbulence model of Transition SST can be used to make predictions about transitions. It combines the SST turbulence model with real-world correlations. This model is commonly known as the SST γ- Reθt transition model. It is designed to handle the transition from laminar to turbulent flow, which is crucial for accurately predicting flow characteristics in various applications, including aerodynamic surfaces and turbine blades.

Several research papers discuss and validate the Transition SST turbulence model. For instance, [22] on a transition model based on correlation utilizing local variables provides foundational information on the development of this model. Another [23] discusses prediction of boundary-layer transition via a simple correlation-based model. The study [24] on the comparison and validation turbulence models for forecasting the wakes of vertically oriented wind turbines also shows that the Transition SST turbulence model is more accurate than the others. [25] also used the same turbulence model in ANSYS Fluent to look at the aerodynamic properties of a NACA 0018 airfoil in a different study. They showed how useful it is in lower Reynolds number. The authors of [26] improved the SST-Reθt transition model to get a better idea of how boundary layer flow changes along curved hydrofoils. They did this by changing the Reynolds number based transition onset based on large eddy simulations (LES) and curvature ratios. The improved model shows superior performance and accuracy in various test cases, making it a valuable tool.

These equations are based on the notion of momentum thickness and Reynolds number (Re). In the turbulence model equation with the symbol γ, is a transport equation used in the laminar area for the intermittency:

$$\frac{\partial(\rho\gamma)}{\partial t} + \nabla.(\rho\gamma v) = G - \rho\alpha f\gamma^2 \qquad (5)$$

G is the intermittency production due to mean velocity gradients, αf is a damping function, and $v$ is the fluid velocity. The model simulates the turbulence in the turbulent zone using a hybrid k-ω turbulence model. The transport equations for the particular dissipation rate (ω) and turbulent kinetic energy (k) are as follows:

$$\frac{\partial(\rho k)}{\partial t} + \nabla(\rho k v) = Pk - \varepsilon + \nabla.(\mu_t \Delta k) \tag{6}$$

$$\frac{\partial(\rho\omega)}{\partial t} + \nabla(\rho\omega v) = P\omega - \beta * \omega^2 + \nabla.(\mu_t \nabla\omega) \tag{7}$$

Where $Pk$ and $P\omega$ are the turbulent production terms, ε is the turbulent dissipation rate, $\mu_t$ is the turbulent viscosity, and β is a constant. Using a blending function based on intermittency, the transition SST model mixes the laminar and turbulent equations to calculate the relative contributions of each area.

Subscale resolving techniques near the wall shear flow for better flow prediction, Stress Blended Eddy Simulation (SBES) is used with the Transition SST model in the simulation model. [27] introduces the SBES model, highlighting its improved shielding properties, rapid RANS-LES transition, and applicability in wall boundary layer flows. The SBES model›s versatility and modularity make it highly attractive for industrial CFD, allowing the unification of many RANS and LES. The model has been successfully applied in ANSYS-Fluent and ANSYS-CFX for various validation cases and complex industrial flows.

## Performance formulation

Performance parameters to be calculated for comparison are Lift to Drag Ratio (L/D)(Aerodynamic Performance) The following are the usual formulas used for calculating the aerodynamic performances,

$$C_l = \frac{F_l}{\frac{1}{2}.\rho.A_{ref}.V^2} \tag{8}$$

$$C_d = \frac{F_d}{\frac{1}{2}.\rho.A_{ref}.V^2} \tag{9}$$

$$\text{L/D} = \frac{C_l}{C_d} \tag{10}$$

Additionally, in this scenario, power consumption for rotating mechanisms has to be considered and included to measure the mechanical effectiveness, η. This procedure was used in [17]. Equations 11, 12, and 13 calculate the coefficient of power consumption, $C_{pow}$ using Coefficient of friction $C_{f,cyl}$ with the shear force $F_{f,Cyl}$ on moving surface and CSR, $\frac{U_c}{U_\infty}$.

$$C_{f,cyl} = \frac{F_{f,cyl}}{\frac{1}{2}.\rho.A_{ref}.U_\infty^2} \tag{11}$$

$$C_{pow} = \frac{F_{f,cyl}.U_c}{\frac{1}{2}.\rho.A_{ref}.U_\infty^3}. = \frac{F_{f,cyl}}{\frac{1}{2}.\rho.A_{ref}.U_\infty^2}.\frac{U_c}{U_\infty} = C_{f,cyl}.\frac{U_c}{U_\infty} = C_{f,cyl}.CSR \tag{12}$$

$$\eta = \frac{C_l}{(C_d + C_{pow})} \tag{13}$$

## Simulation Setup

The viscous fluid flow is assumed for incompressible (M = 0.099) and turbulent (Re = 2.2x10$^6$) flow. The domain has been modeled with a standard C section at the front and rectangular at the back, with a size of 15C from the model under analysis in all directions. Flow conditions are maintained at

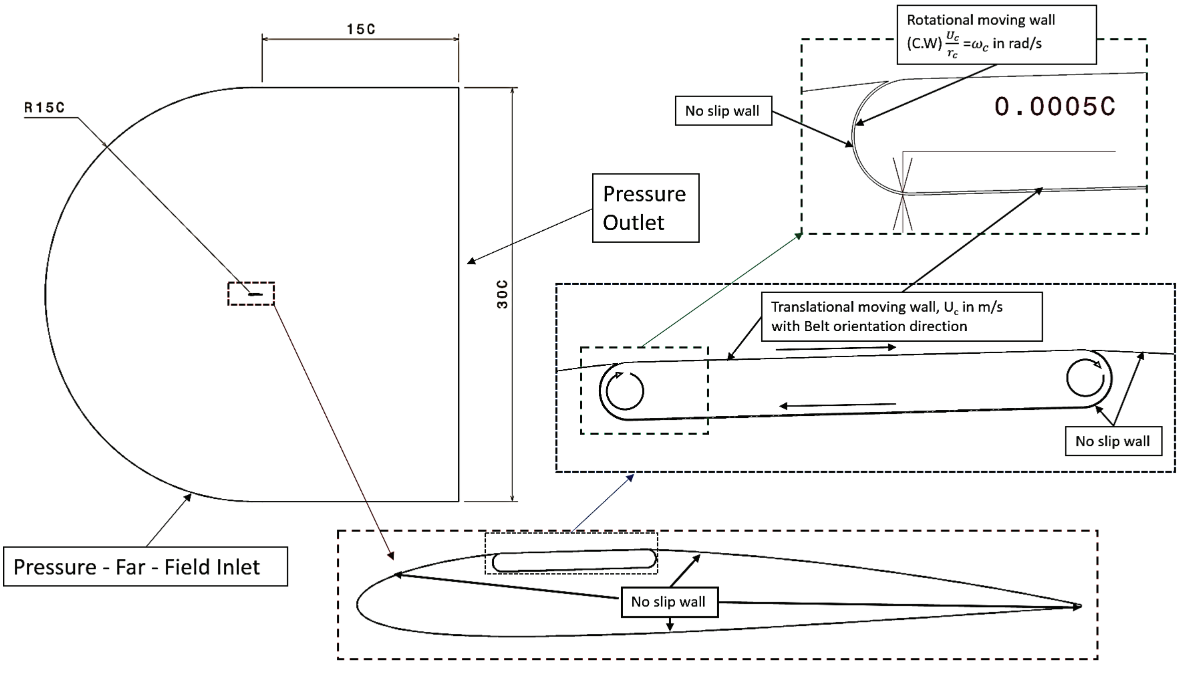

**Figure 2.** Domain setup and boundary conditions.

**Table 1.** Grid independence study

| S.No. | at Airfoil's LE | | | | MP at 0.2C | | | | MP at 0.4C | | | |
|---|---|---|---|---|---|---|---|---|---|---|---|---|
| | No. of Elements (in millions) | Cl | Cd | L/D | No. of Elements (in millions) | Cl | Cd | L/D | No. of Elements (in millions) | Cl | Cd | L/D |
| 1 | 0.13 | 1.16 | 0.0573 | 20.27 | 0.11 | 1.71 | 0.0275 | 62.27 | 0.12 | 1.62 | 0.0265 | 61.29 |
| 2 | 0.26 | 1.70 | 0.0258 | 65.82 | 0.23 | 1.67 | 0.0278 | 60.08 | 0.25 | 1.63 | 0.0286 | 57.19 |
| 3 | 0.53 | 1.69 | 0.0256 | 66.02 | 0.46 | 1.67 | 0.0277 | 60.22 | 0.48 | 1.64 | 0.0285 | 57.69 |

sea level where the free stream temperature is room temperature (T = 300K), the air density at the given temperature is $\rho = 1.177$ kg/m$^3$, and the viscosity is $\mu = 1.846\times10^{-5}$ kg/m.s correspondingly. The energy equation is used to get accurate solutions as the flow is accelerated. Figure 2 describes the domain and boundary conditions for NACA 2412 with MP's LE at 0.2C, which is similar to the other models.

### Grid Generation and Grid Independence

A structured grid for the modified airfoil with MP at 0.2C can be seen in Figure 3. It is developed using the blocking method, and we were able to make a refined mesh where the grid cell size of y+ stays below 1 near the wall surface and stays relatively coarse in the free stream region. The grid independence has been conducted for each model as listed in Table 1.

### Validation

The benchmark study has been conducted with Base NACA 2412 Airfoil, similar to the condition performed experimentally [28]. The study has been performed at Re=2.2x10$^6$ and aerodynamic performances and flow separations were compared as shown in Figure 4.

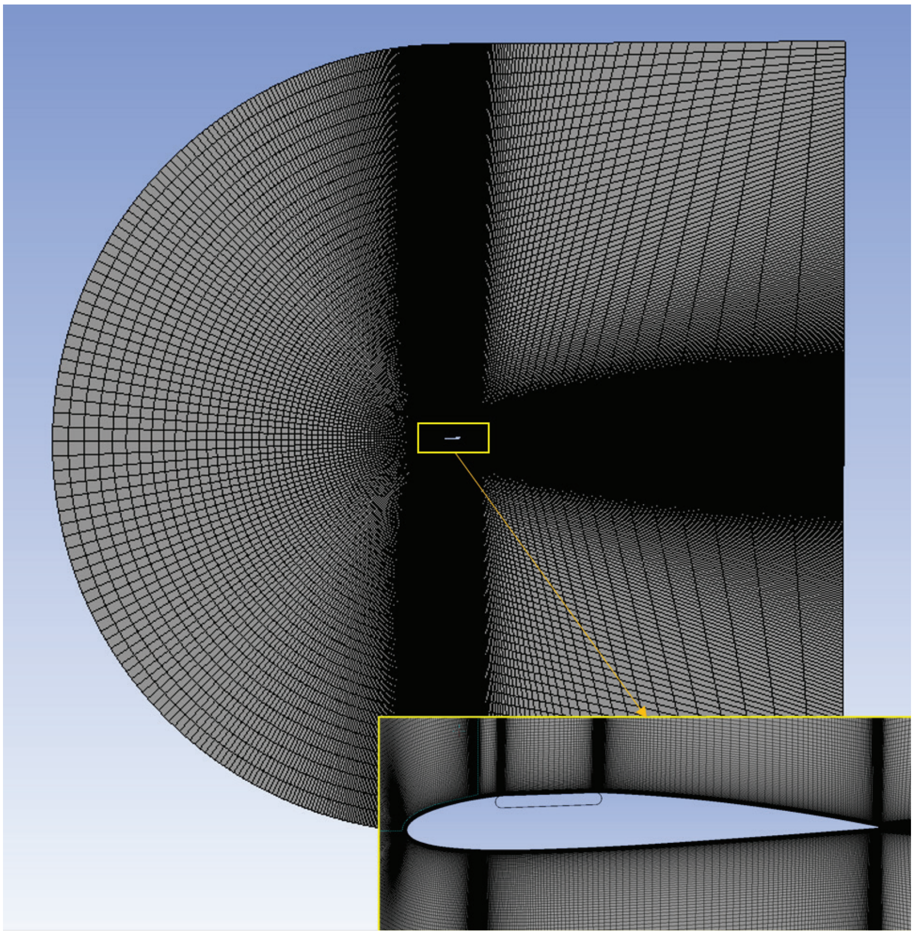

**Figure 3.** Grid layout.

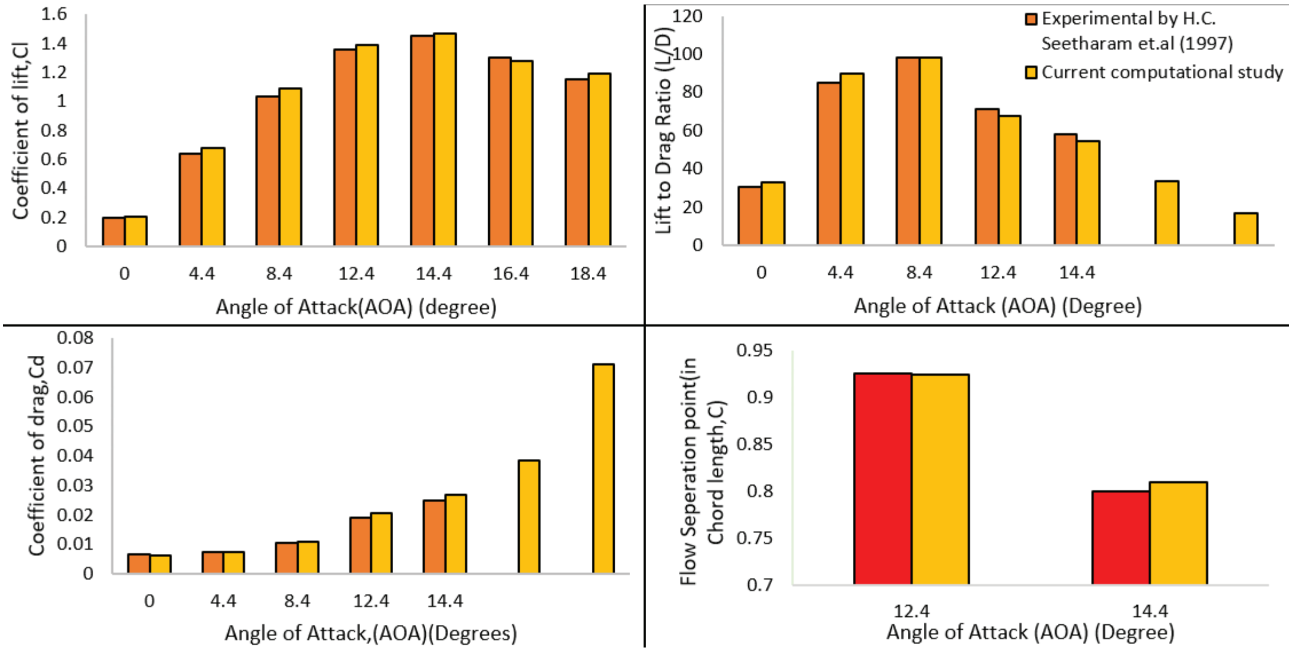

**Figure 4.** Flow setup validation.

The prediction is accurate up to the flow separation's stall angle, which is less than 1%. The predictions of stall and coefficients of lift and drag are in acceptance range compared with experimental reference.

## RESULTS AND DISCUSSION

Simulations were conducted for the NACA2412 airfoil with the MP›s LE positioned at three different locations: at the airfoil›s LE, 0.2C (20% chord length), and 0.4C (40% chord length) as shown in Figure 5. Each simulation included either a 0.025 CD cylinder or a roller with two numbers. The cylinder or roller had a CSR value of 0, 1, 2, or 3. In each simulation, the airfoil was studied at various AOA until the post-stall angle was detected. After obtaining grid independence, the coefficient of lift, aerodynamic performance (L/D), and mechanical effectiveness (η) were compared and studied for each CSR and AOA.

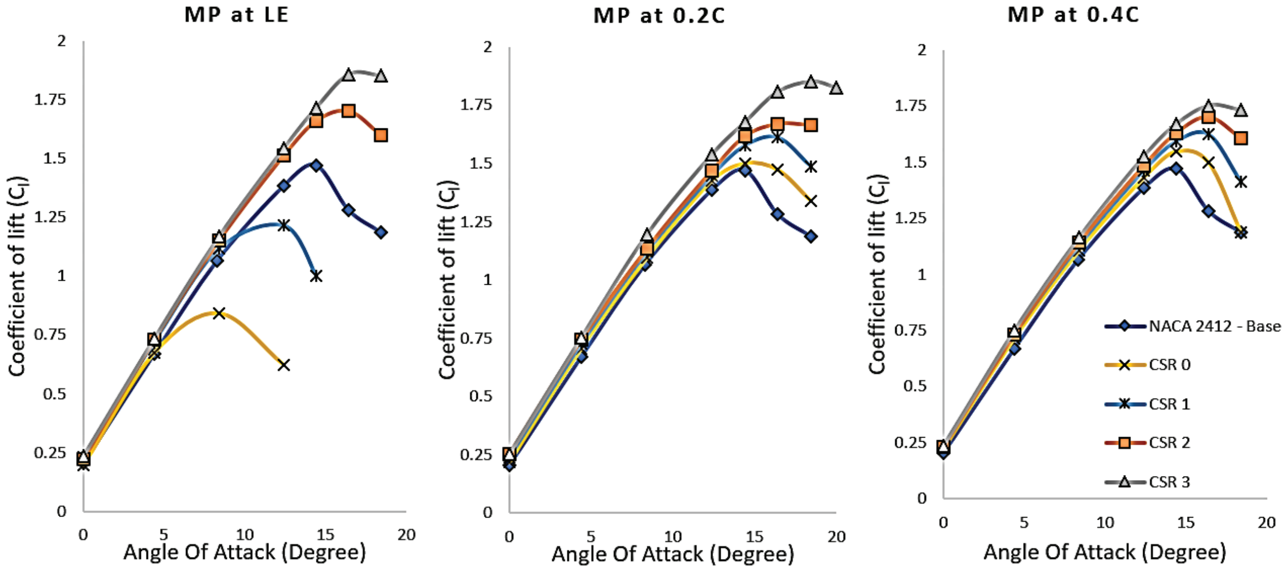

**Figure 5.** Generation of lift.

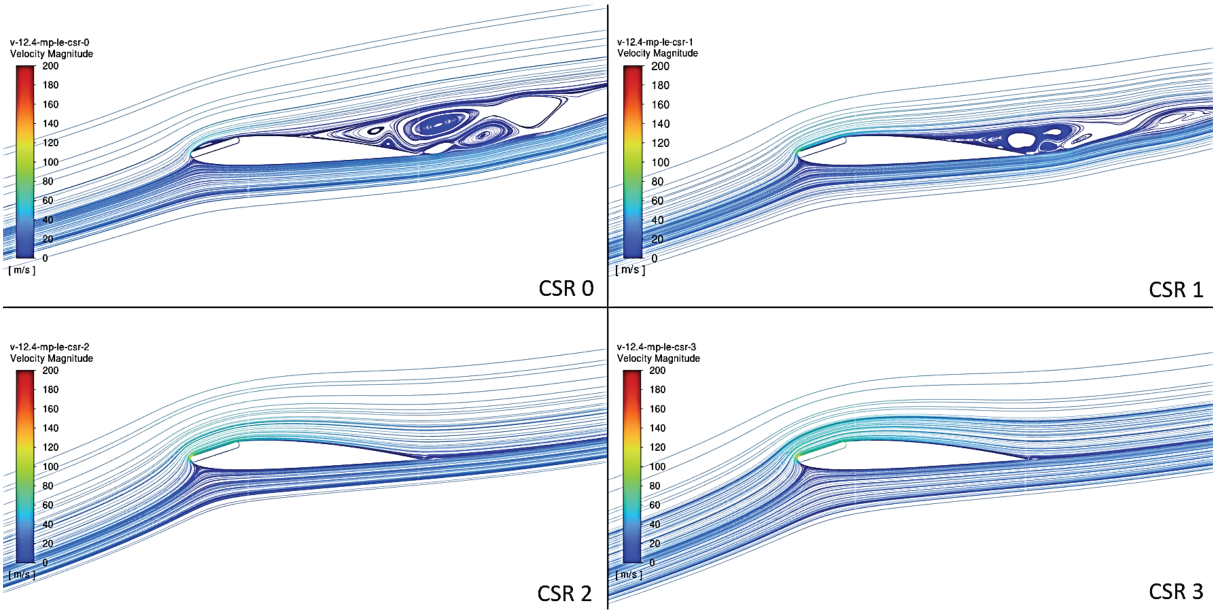

**Figure 6.** Streamline plot of NACA 2412 with MP at LE at 12.4°.

## Generation of Lift

The models have been simulated for various AOAs from 0° until the post-stall angle was reached for each CSR and plotted along with NACA 2412 – Base in Figure 6. The MP configurations at 0.2C and 0.4C demonstrate a more stable, consistent, and linear improvement in lift across all CSRs. Regarding stall angle, the MP at 0.2C achieves the highest stall angle of 18.4°, with a maximum lift coefficient (Cl, max) of 1.85 at CSR 3. Other CSRs for this configuration achieve a stall angle of 16.4°. In the post-stall regime, it exhibits a smoother decline in lift compared to the sharper drop-offs seen in other configurations. The MP at LE shows significant variation in stall angles between CSRs, with a maximum Cl of 1.86 at a stall angle of 16.4° at CSR 3. Meanwhile, the MP at 0.4C maintains a consistent stall angle of 16.4° across all CSRs. Overall, the MP at 0.2C demonstrates the best lift characteristics among the three configurations, offering both high lift and a smoother decline in performance after stalling.

## Aerodynamic Efficiency (L/D Ratio)

The L/D ratio is crucial for aerodynamic performance, encompassing both lift and drag components. In Figure 7, three graphs (a, b, and c) illustrate the L/D ratio for the NACA 2412 airfoil with the MP at the airfoil's LE, 0.2C, and

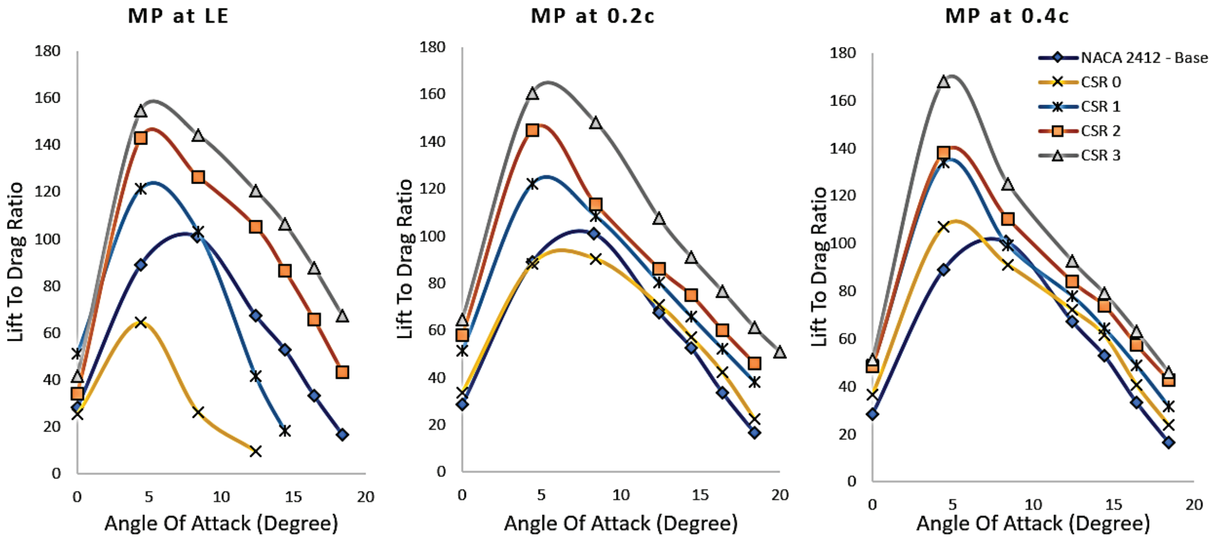

**Figure 7.** Comparison of aerodynamic performance (lift to drag ratio).

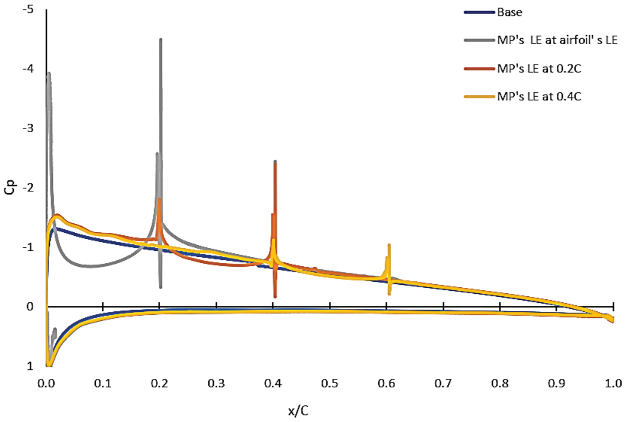

**Figure 8.** Coefficient of pressure distribution comparison for 4.4° at CSR 3.

0.4C, respectively, across a range of AOAs and CSRs. At 0°, the MP at 0.2C outperforms the other configurations, while the MP at the airfoil's LE exhibits the lowest performance, and the MP at 0.4C shows intermediate results. Around 4°, all three MP locations achieve maximum aerodynamic efficiency for their respective CSRs, with the MP at 0.4C exhibiting the highest efficiency at CSR 3.

Figure 8 indicates that all MP models have a superior Cp distribution compared to the baseline. The farther the MP is positioned from the LE (0.2C and 0.4C), the less severe the pressure spikes, suggesting more controlled flow behavior. [17] provides a simplified flat moving surface representation that may account for the absence of these spikes in Cp distribution due to omitting the belt system. Notably, the MP at 0.4C demonstrates better Cp distribution with minimal loss compared to other configurations.

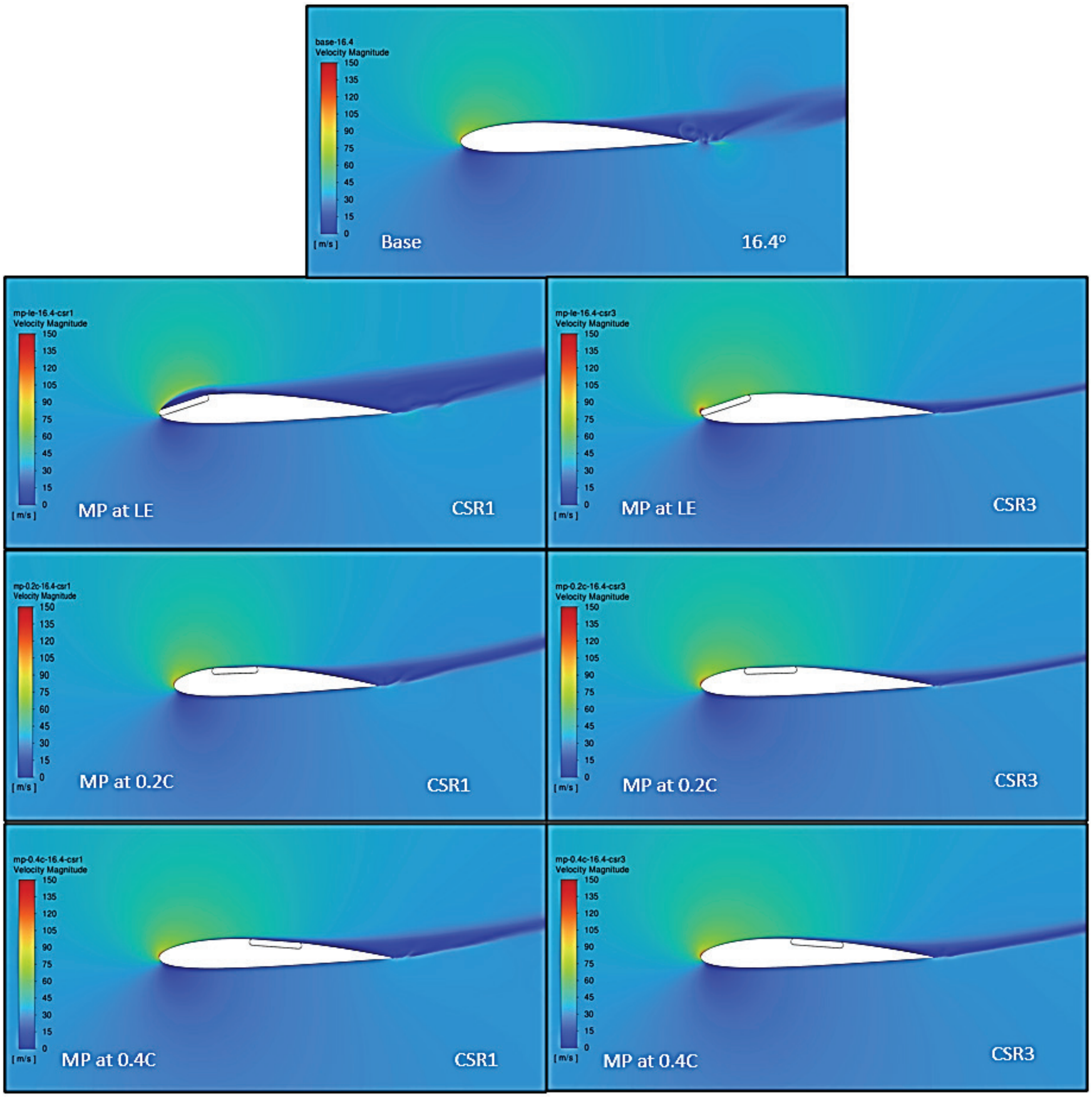

**Figure 9.** Comparison of velocity contour of NACA2412 at 16.4° for CSR 1 and 3.

Beyond 4.4°, the MP at the airfoil's LE shows improved aerodynamic efficiency at CSRs 2 and 3. After reaching peak efficiency, the rate of improvement slows as the CSR increases and the MP moves farther from the LE. Figure 9 reveals that flow separation decreases with higher CSRs, regardless of the MP's location. When positioned farther from the LE, the MP performs better at lower AOAs, achieving optimal aerodynamic performance. Conversely,

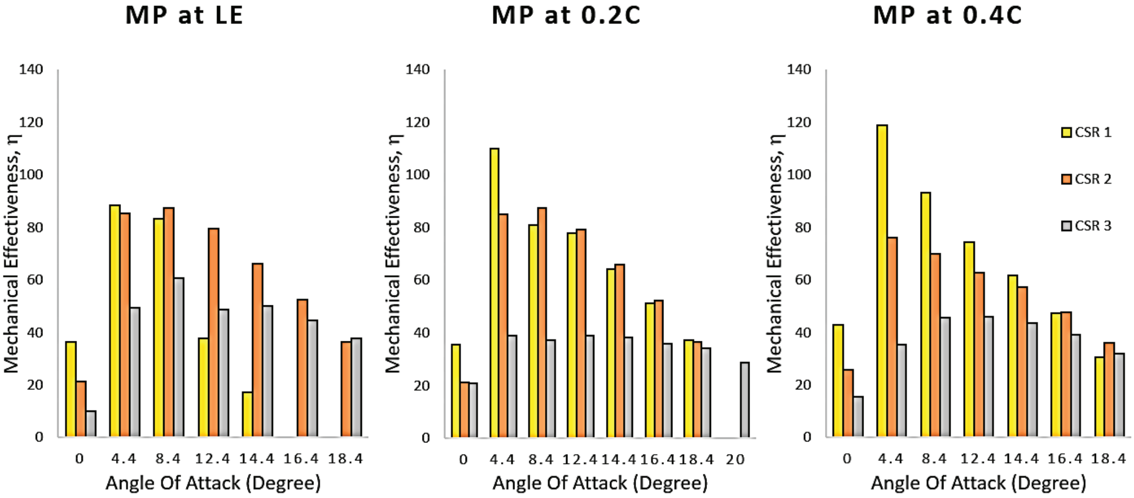

**Figure 10.** Comparison of mechanical effectiveness.

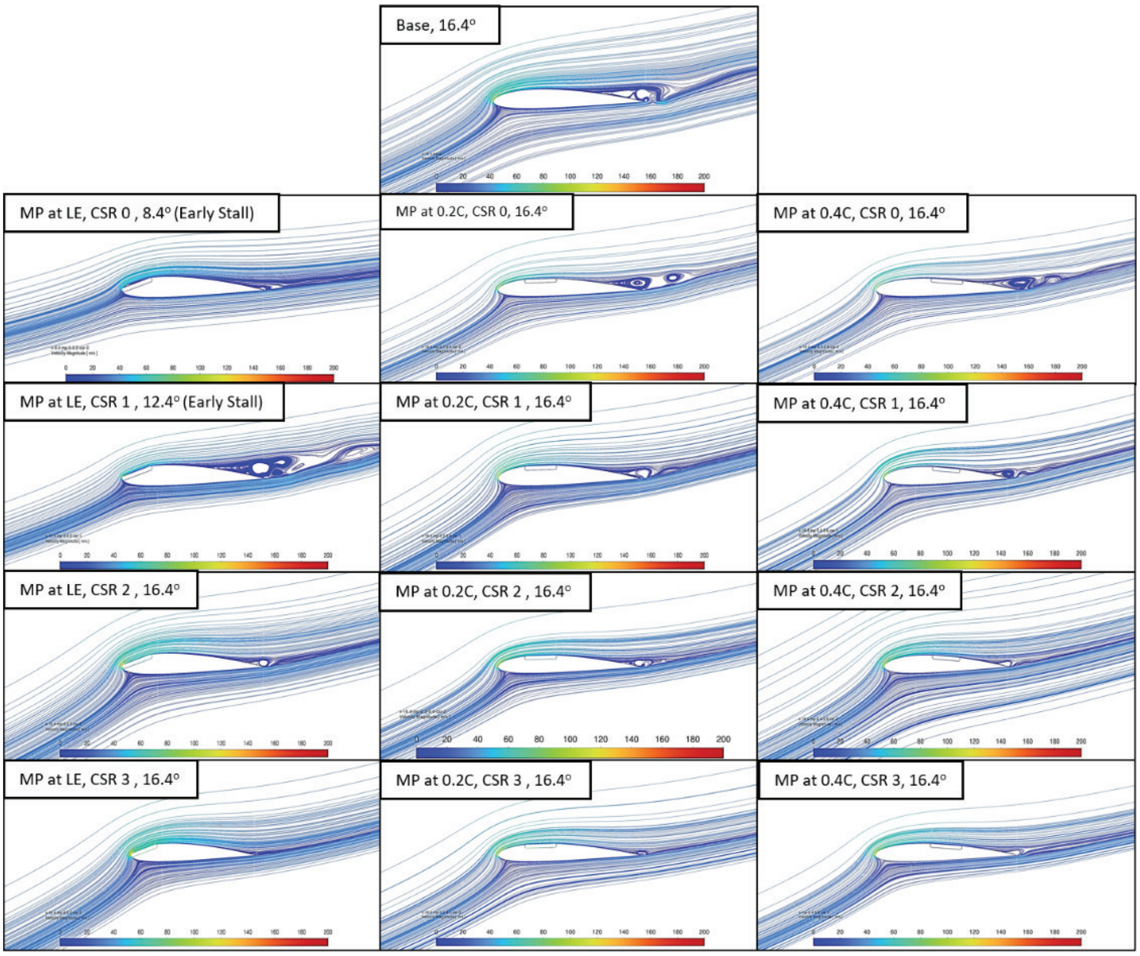

**Figure 11.** Streamlined plots at 16.4°.

at higher AOAs, the MP performs best when positioned closer to the LE.

### Mechanical Effectiveness

Mechanical effectiveness (η) is measured as an additional parameter to account for the power consumption of the MP, included as the wall shear drag component in the L/D ratio. This formulation, outlined in equations (11), (12), and (13), helps determine the overall effectiveness of the mechanism and the CSR configuration. Higher mechanical effectiveness indicates lower power consumption, resulting in more lift and less drag.

Figure 10 illustrates this comparison for CSR 1, 2, and 3 across all three MP configurations. Overall, CSR 1 demonstrates high mechanical effectiveness from 0° to 4.4° across all configurations. CSR 2 is more effective in the mid-range (8.4° to 16.4°) for the MP at the LE and at 0.2C. However, for the MP at 0.4C, CSR 1 remains the most effective compared to CSR 2 and 3. These findings align with those reported by [17]. At lower AOA, mechanical efficiency is higher at lower CSRs. As the AOA increases, higher CSRs contribute to better mechanical efficiency. Furthermore, as the MP is positioned farther from the LE, the effectiveness of each CSR decreases more gradually.

### Delay of Flow Separations at Stall Angles

In the NACA 2412 base configuration, the stall angle reached 14.4°. In contrast, all three modified configurations achieved a highest stall angle of approximately 16° and beyond it. Figure 11 compares the flow patterns at 16.4° for all models across different CSRs. For the MP at the LE, CSR 0 and 1 exhibited early stalls at 8.4° and 12.4°, respectively. In CSR 0, the separation bubble at the MP may destabilize the flow and induce more drag. In CSR 1, flow separation is characterized by a large recirculation zone and the formation of a vortex behind the airfoil.

As the CSR increases to 2 and 3, the stall angle extends to 16.4°, indicating delayed flow separation and minimized recirculation. For the MP at 0.2C, the stall angle remains at 16.4° across all CSRs. Recirculation is substantial at CSR 0, but flow separation is suppressed and delayed as the CSR increases from 0 to 3. A similar performance trend is observed in the MP at 0.4C.

## CONCLUSION

The analysis reveals that positioning the moving panel at 20% of the chord length delivers the best overall performance in terms of lift generation, aerodynamic efficiency, and mechanical effectiveness. This configuration produces higher lift, with a stall angle of 18.4° at a cylinder speed ratio of 3, compared to a 16.4° stall in other setups. Although the highest aerodynamic efficiency (lift-to-drag ratio of 168) is achieved with the panel positioned at 40% of the chord, the panel at 20% delivers superior performance at higher angles of attack, achieving a lift-to-drag ratio of 160.

For mechanical efficiency, the cylinder speed ratio of 1 is optimal at low attack angles (0° to 4°), while a ratio of 2 performs best at mid-range angles (8° to 16°). As the angle of attack increases beyond 4.4°, the mechanical efficiency of all cylinder speed ratios decreases, though this effect stabilizes when the moving panel is placed farther from the leading edge. The 20% chord position shows improved performance at higher speed ratios, though it does not consistently outperform other configurations at lower ratios.

This study demonstrates that integrating a moving panel at 20% of the chord, combined with appropriate cylinder speed ratios, provides significant improvements in aerodynamic performance. This approach offers valuable insights for optimizing lift and efficiency in applications such as aircraft wings, wind turbine blades, and automotive aerodynamic surfaces. Due to its adaptability across different attack angles and speed ratios, this method holds great potential for enhancing stability and performance in high-performance vehicles and control surfaces.

### Future Scope

The findings offer valuable insights into the behavior of belt-type moving surface mechanisms along the chordwise direction. Future research could extend this analysis to the spanwise direction using a 3D model, enabling a more comprehensive performance evaluation. Additionally, experimental studies could be conducted to validate the numerical results and uncover further insights.

## NOMENCLATURE

| | |
|---|---|
| AOA | Angle of Attack |
| C | Chord |
| CSR | Cylinder Speed Ratio |
| MP | Moving Panel |
| M | Mach number |
| Re | Reynold's number |
| SST | Shear Stress Transport |
| LE | Leading Edge |
| $k$ | Kinetic Energy of turbulence (J/kg) |
| $\omega$ | Specific Dissipation rate of turbulence ($m^2/s^3$) |
| $U_\infty$ | Free Stream Velocity (m/s) |
| Uc | Cylinder Tangential Velocity (m/s) |
| $C_l$ | Coefficient of Lift (-) |
| $C_d$ | Coefficient of Drag (-) |
| Re | Reynolds number (-) |
| u | Velocity in x- direction (m/s) |
| v | Velocity in y- direction (m/s) |
| t | time (s) |
| μ | Dynamic Viscosity (kg/ (m.s)) |
| Su, Sv and $S_T$ | Source Terms |
| ρ | Density of air ($kg/m^3$) |
| $C_p$ | Specific heat at constant pressure (J/ (kg. K) |
| T | Temperature (K) |
| $k_T$ | Thermal conductivity (W/ ($m^2$.K)) |

| | |
|---|---|
| G | Intermittency Production due to mean velocity gradients |
| αf | damping function |
| $\gamma$ | intermittency in the laminar region; |
| $P_k$ and $P_\omega$ | turbulent production terms; |
| $\varepsilon$ | turbulent dissipation rate($m^2/s^3$) |
| $\mu_t$ | turbulent viscosity |
| $\beta$ | constant; and |
| $C_f$ | Skin friction coefficient |
| $U_c/U_\infty$ | Cylinder Speed Ratio |
| $C_{pow}$ | *coefficient of power consumption* |
| $C_{f,cyl}$ | Coefficient of friction on moving surface |
| $F_{f,Cyl}$ | Shear force on moving surface |
| $\eta$ | Mechanical Effectiveness |

## AUTHORSHIP CONTRIBUTIONS

Authors equally contributed to this work.

## DATA AVAILABILITY STATEMENT

The authors confirm that the data that supports the findings of this study are available within the article. Raw data that support the finding of this study are available from the corresponding author, upon reasonable request.

## CONFLICT OF INTEREST

The authors declared no potential conflicts of interest with respect to the research, authorship, and/or publication of this article.

## ETHICS

There are no ethical issues with the publication of this manuscript.

## REFERENCES

[1] Johnson WS, Tennant JS, Stamps RE. Leading-edge rotating cylinder for boundary-layer control on lifting surfaces. J Hydronautics 1975;9:76–78. [CrossRef]

[2] Moktarian F, Modi VJ. Fluid dynamics of airfoils with moving surface boundary-layer control. J Aircr 1988;25:163–169. [CrossRef]

[3] Modi VJ, Fernando MSUK, Yokomizo T. Moving surface boundary-layer control: Studies with bluff bodies and application. AIAA Journal 1991;29:1400–1406. [CrossRef]

[4] Den Hertog VR. Moving surface boundary-layer control with application to autonomous underwater vehicles [dissertation]. University of British Columbia; 1999.

[5] Du X, Lee T, Mokhtarian F, Kafyeke F. Flow past an airfoil with a leading-edge rotation cylinder. J Aircr 2002;39:1079–1084. [CrossRef]

[6] Ekaterinaris JA. Prediction of active flow control performance on airfoils and wings. Aerosp Sci Technol 2004;8:401–410. [CrossRef]

[7] Robson SE, Ahmedp NA. Drag reduction on bluff bodies using a rotating device. 15th Australasian Fluid Mechanics Conference, University of Sydney, Sydney, Australia, 13-17 December 2004.

[8] Aktharuzzaman M, Sarker MS, Safa W, Sharah N, Salam MA. Development of an experimental setup for analyzing the influence of Magnus effect on the performance of airfoil. AIP Conf Proc 2017;1919:5018550. [CrossRef]

[9] Islam MS, Hakim SM, Ali M, Islam MQ. Numerical investigation on boundary layer control through moving surface in NACA 0012 airfoil. AIP Conf Proc 2017;1851:4984740. [CrossRef]

[10] Naik SN, Vengadesan S, Prakash KA. Numerical study of fluid flow past a rotating elliptic cylinder. J Fluids Struct 2017;68:15–31. [CrossRef]

[11] Patel V, Parekh S, Parwani AK. Numerical simulation of moving surface boundary-layer control over symmetric aerofoil. In: Parwani A, Ramkumar P, eds. Recent Advances in Mechanical Infrastructure. Lecture Notes in Intelligent Transportation and Infrastructure. Singapore: Springer; 2020. pp. 225–234. [CrossRef]

[12] Ali HM, Rafie ASM, Ali SAM, Gires E. Computational analysis of the rotating cylinder embedment onto flat plate. CFD Letters 2021;13:133–149. [CrossRef]

[13] Zhang Y, Zhao Y. Novel design of a circulation control airfoil with cylinder rotation. Phys Fluids 2023;35:0158974. [CrossRef]

[14] Zhang Y, Huang D, Sun X, Wu G. Exploration in optimal design of an airfoil with a leading edge rotating cylinder. J Therm Sci 2010;19:318–325. [CrossRef]

[15] Zhuang Y, Sun X, Huang D, Wu G. Numerical study on aerodynamic performances of the wind turbine rotor with leading-edge rotation. J Renew Sustain Energy 2012;4:4765697. [CrossRef]

[16] Amin Boukenkoul M, Li FC, Chen WL, Zhang HN. Lift-generation and moving-wall flow control over a low aspect ratio airfoil. J Fluids Eng 2018;140:4037681. [CrossRef]

[17] Salimipour E. On the moving surface impact on flow field and aerodynamic performance of a thick airfoil. Ocean Engineer 2024;291:116504. [CrossRef]

[18] Salimipour E, Yazdani S. Improvement of aerodynamic performance of an offshore wind turbine blade by moving surface mechanism. Ocean Engineer 2020;195:106710. [CrossRef]

[19] Salimipour E, Dayani H. Investigating the characteristics of flow past an elliptic moving belt. Ocean Engineer 2023;267:113296. [CrossRef]

[20] Salimipour E, Salimipour A. Power minimization and vortex shedding elimination of a circular cylinder by moving surface mechanism. Ocean Engineer 2019;189:106408. [CrossRef]

[21] Salimipour E, Yazdani S, Ghalambaz M. Flow field analysis of an elliptical moving belt in transitional flow regime. Eur Phys J Plus 2021;136:783. [CrossRef]

[22] Menter FR, Langtry RB, Likki SR, Suzen YB, Huang PG, Völker S. A correlation-based transition model using local variables—part I: Model formulation. J Turbomach 2006;128:413. [CrossRef]

[23] Xia C, Chen W. Boundary-layer transition prediction using a simplified correlation-based model. Chinese J Aeronaut 2016;29:66–75. [CrossRef]

[24] Barnes A, Marshall-Cross D, Hughes BR. Validation and comparison of turbulence models for predicting wakes of vertical axis wind turbines. J Ocean Eng Mar Energy 2021;7:339–362. [CrossRef]

[25] Michna J, Rogowski K. Numerical study of the effect of the reynolds number and the turbulence intensity on the performance of the NACA 0018 airfoil at the low Reynolds number regime. Processes 2022;10:1004. [CrossRef]

[26] Ye C, Wang C, Zi D, Tang Y, van Esch BartPM, Wang F. Improvement of the SST γ-Reθt transition model for flows along a curved hydrofoil. J Hydrodynamics 2021;33:520–533. [CrossRef]

[27] Menter F. Stress-Blended Eddy Simulation (SBES)—a new paradigm in hybrid RANS-LES modeling. In: Hoarau Y, Peng SH, Schwamborn D, Revell A, eds. Progress in Hybrid RANS-LES Modelling. HRLM 2016. Notes on Numerical Fluid Mechanics and Multidisciplinary Design, vol 137. Cham; Springer; 2018. [CrossRef]

[28] Seetharam HC, Rodgers EJ, Wentz WH Jr. Experimental studies of flow separation of the NACA 2412 airfoil at low speeds. Aeronautical Report 77-3. NASA-CR-197497; 1977.

[29] Modi VJ, Mokhtarian F, Fernando MSUK, Yokomizo T. Moving surface boundary-layer control as applied to two-dimensional airfoils. J Aircr 1991;28:104–112. [CrossRef]